applied sciences

MDPI

Article

Experimental Study of Ultrasound-Assisted Reaming of Carbon Fiber-Reinforced Plastics/Titanium Alloy Stacks

Shengtong Liu, Renke Kang, Yan Qin, Zhigang Dong, Xiaoguang Guo and Yidan Wang *

State Key Laboratory of High-Performance Precision Manufacturing, Liaoning Province, Dalian University of Technology, Dalian 116024, China
* Correspondence: ydwang@dlut.edu.cn

Abstract: Carbon fiber-reinforced plastic/titanium alloy (CFRP/Ti) stacks are widely used in the aerospace field based on their high strength to weight ratio and heat resistance. High-quality bolt hole assembly is critical for the safety of the aerospace industry. Reaming is a crucial process in precision machining and is extensively used to improve the quality of bolt holes. Due to the different properties of the material, machining with conventional reaming (CR) presents some challenges, such as tolerance variations across the hole group and difficulty in controlling thrust. In this paper, ultrasonic vibration is applied to the reaming process. A geometrical model of ultrasonic vibration reaming (UVR) was established to analyze its kinematic law. UVR experiments on CFRP/Ti stacks were carried out to study the influence of different ultrasonic amplitudes on reaming thrust and the influence of tool speed on thrust, dimensional accuracy, and surface roughness under optimal ultrasonic amplitude. The average thrust forces in UVR decreased by over 57% (Ti) and 40% (CFRP), respectively, compared to CR. The roughness of CFRP is reduced by 20% with UVR and 28% for titanium alloys. The surface topography of the holes is significantly improved by UVR. This work guides the manufacture of high-quality bolt holes for CFRP/Ti stacks.

Keywords: CFRP/Ti stacks; ultrasonic vibration reaming; thrust force; surface finish

check for updates

Citation: Liu, S.; Kang, R.; Qin, Y.; Dong, Z.; Guo, X.; Wang, Y. Experimental Study of Ultrasound-Assisted Reaming of Carbon Fiber-Reinforced Plastics/Titanium Alloy Stacks. *Appl. Sci.* **2023**, *13*, 5309. https://doi.org/10.3390/app13095309

Academic Editors: Wendong Xiao, Jin Guo and Wei Su

Received: 20 March 2023
Revised: 16 April 2023
Accepted: 20 April 2023
Published: 24 April 2023

Copyright: © 2023 by the authors. Licensee MDPI, Basel, Switzerland. This article is an open access article distributed under the terms and conditions of the Creative Commons Attribution (CC BY) license (https://creativecommons.org/licenses/by/4.0/).

1. Introduction

Carbon fiber-reinforced plastic/titanium alloy (CFRP/Ti) stacks are widely used as joint components with a high load-bearing capacity in the wings and fuselages of aircrafts [1–4]. CFRP/Ti stacks possess not only the advantages of CFRP [5], such as high specific strength, good vibration damping, and good fatigue resistance, but also the advantages of titanium alloys [6], such as superior strength, low density, excellent hardness, good corrosion resistance, extreme temperature resistance, etc. As a result, with the effects of improving the overall strength and achieving the lightweight demand, CFRP/Ti stacks have gradually replaced traditional alloy materials in the advanced aircraft manufacturing industry.

Laminated material components are usually fastened via bolt holes, which determine the assembly strength and become vital to flight safety [7]. Aircraft assembly requires extremely high-quality bolt holes, particularly holes that cannot be damaged. As both CFRP and titanium alloys are typical difficult-to-machine materials, the laminated materials prepared from them will face new challenges when machining. CFRP is highly susceptible to defects such as delamination and tearing with conventional drilling [8]. In contrast, titanium alloys are prone to defects such as chipping at the entrance and burrs at the exit. The hole quality from conventional drilling cannot satisfy aircraft assembly requirements. Therefore, reaming finishing of bolt holes is indispensable [9,10].

Reaming is the process of removing a very thin layer of material from the hole wall with a reamer to improve dimensional accuracy and surface quality. However, the bolt holes of CFRP/Ti stacks made by the existing reaming process still cannot reach the excellent

tolerance requirement [11–16]. Moreover, other problems also exist. The dimension of the machined diameter and roundness is unstable. The hole entrance of CFRP materials is prone to burrs, while residual damage may appear at the hole exit. This can harm the stack's mechanical integrity with negative effects such as the loosening of bolted connections.

Ultrasonic-assisted drilling has been widely focused on by researchers in recent years due to its advantages of low thrust forces and enhanced surface quality. Cong et al. [17] drilled CFRP/Ti stacks with variable feed rate machining and concluded that drilling stacks with variable feed rates (low feedrate should be used for machining of Ti, and machining of CFRP could be conducted using feedrate 10 times higher) at different ultrasonic output powers resulted in lower axial forces than with fixed feed rates. In addition, the cycle time using variable feedrate was shorter than that using fixed federate, which led to lower tool wear. Gao et al. [18] carried out an experimental study of the ultrasonic vibration-assisted helical milling drilling process for laminated composites and found that ultrasonic vibration-assisted helical milling reduces thrust forces, hole exit tears, burrs, and other defects. Ma et al. [19–21] drilled CFRP with ultrasonic longitudinal and torsional vibration, which reduced the thrust forces and hole exit burrs and reduced the surface roughness of the hole wall due to the torsional vibration of the side edge of the drill in longitudinal, and torsional vibration helps strengthen the effect of resin adhesion. It has been proven that the variable stress state makes the fibers more susceptible to shear fracture by kinematic characteristic analysis. Geng et al. [22] introduced ultrasonic elliptical vibration-assisted reaming into finish drilling CFRP/Ti stacked bolt holes and showed that it can reduce axial forces and torques, where the average axial force can be reduced by 30%, and the geometric accuracy of the hole is better compared to conventional reaming (CR). In dry reaming, it is of great value to select ultrasonic power and cutting parameters quickly for efficient practical machining. Research shows that ultrasonic-assisted machining can reduce axial force and improve machining quality in reaming, but the effect of reducing axial force with different output power is not specified, which of guiding significance for industrial practice. In CR, the influence rule of different cutting conditions on dry reaming is that it is advantageous for the operator to choose the appropriate processing parameters, which is also the same in ultrasonic reaming. There are now some guiding machining parameters with cutting fluids added, but there is no guiding conclusion on the cutting parameters with dry conditions. However, during the reaming of CFRP/Ti stacked holes, there is little research on the influence of CR and UVR on the axial force and surface quality during reaming. Furthermore, there has been no systematic study on the impact of cutting conditions on the quality of reaming in CR and UVR.

In this paper, based on the motion characteristics analysis of ultrasonic vibration reaming (UVR), UVR experiments are conducted on CFRP/Ti stacks to explore the thrust forces, hole wall roughness, hole entrance and exit surface topography, hole diameter, and roundness with the variation of tool speed. In addition, it is verified that ultrasonic reaming can reduce the thrust forces and improve the hole quality, which can provide guidance for high-quality hole-making of CFRP/Ti stacks.

2. Experiments

The experimental setup diagram of UVR for CFRP/Ti stacks is shown in Figure 1a. The adopted experimental platform is a 5-axis vertical machine center (KMC600SU, Kede Machine Tool Co., Ltd., Dalian, China), which includes the UVR unit and the thrust forces measurement unit, as shown in Figure 1b. The UVR unit consists of an ultrasonic generator, a UAR tool holder, and a carbide reamer. The ultrasonic generator converts conventional (220 v, 50 Hz AC) power into high-frequency electrical energy, which will supply the piezoelectric transducer. The piezoelectric transducer converts the high-frequency electrical energy into mechanical vibrations. The ultrasonic vibrations from the transducer are amplified and transmitted to the reamer, which causes the reamer to vibrate axially at high frequency. It has been proven that the greater the output power, the greater the amplitude.

The amplitude of the ultrasonic vibrations can be adjusted by varying the output power of the power supply.

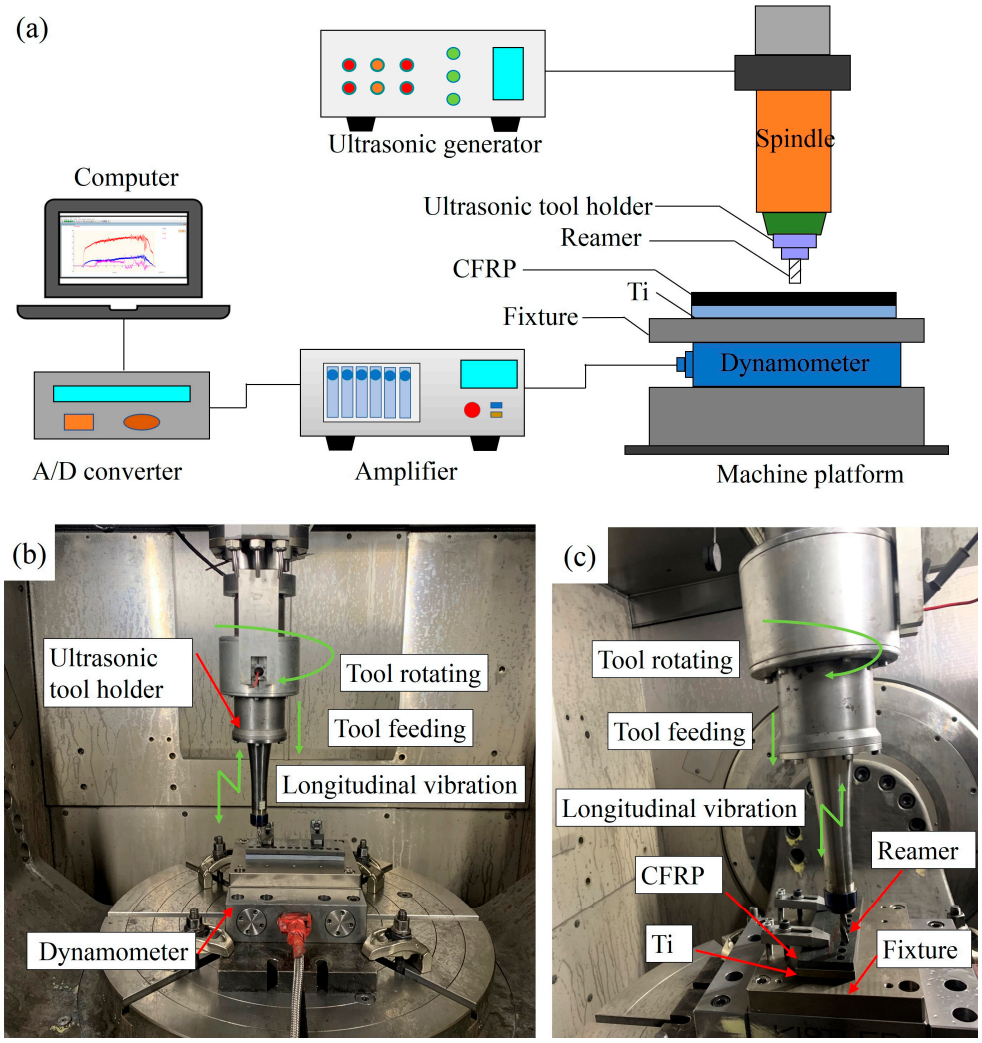

Figure 1. Experimental setup: (**a**) the schematic diagram; (**b**) the overall view of platform; (**c**) the side view of platform.

The experimental materials are CFRP (T700-12K/AG80) and titanium alloy (Ti6AI4V) stacks, where CFRP plate and titanium alloy plate are glued together, as shown in Figure 1c. CFRP is at the top and titanium is at the bottom. This stacking method is a common stacking sequence in industry. When the CFRP is at the bottom and the titanium alloy is at the top, the tool passes through the titanium alloy at a high temperature and cokes the CFRP at the bottom. According to the company's requirements, the top CFRP is being placed and the bottom titanium alloy is being placed. This is a commonly used direction for titanium alloys in industry. The thicknesses of the CFRP and the titanium alloy are 7 mm and 8 mm, respectively. The reason for the different thicknesses is that they are bonded with glue in the middle, close to 1 mm, similar to the CFRP bonding method, which is essential to ensure the same thickness of the two layers. The fiber laying direction of CFRP is 0° and 90°, and the stacking order is $0/90/0_5/90/0_{2s}$. The main component of CFRP is carbon fiber, and its resin matrix is epoxy resin. The CFRP plate is placed on the top of the titanium alloy plate, and their compositions and performance parameters are shown in Tables 1–4.

Table 1. Compositions of T700-12K/AG80 CFRP.

Item	Material Grades	Substrate Material	Pavement	Fiber Volume Fraction/%	Fiber Bundles
Value	T700	AG80	10 layers	60	6 μm,12 K

Table 2. Properties of T700-12K/AG80 CFRP.

Item	Value
Density/(g·cm^{-3})	1.55
Transverse modulus of elasticity/GPa	40
Longitudinal modulus of elasticity/GPa	230
Main Poisson's ratio	0.26
Transverse shear modulus/GPa	14.3
Longitudinal shear modulus/GPa	24
Longitudinal tensile strength/MPa	4900

Table 3. Chemical compositions of Ti6AI4V alloy.

Element	Al	V	Fe	O	C	N	H	Ti
Content/wt%	5.5–6.75	3.5–4.5	<0.25	<0.2	<0.88	<0.05	<0.01	Residuals

Table 4. Properties of Ti6Al4V.

Item	Value
Density/(g·cm^{-3})	4.4
Modulus of elasticity/GPa	109
Tensile strength/Mpa	950
Poisson's ratio	0.34
Elongation/%	8
Hardness/HV	360

A 4-fluted carbide reamer (Figure 2) with a diameter of D 7.8 mm ± 0.003 mm and a helix angle of 18° was used in the experiment. Titanium alloys have high chip hardness and slenderness, making it very easy to scratch the reamed CFRP holes. In order to avoid secondary scratches on CFRP holes caused by chips discharged during reaming, only the left helical-edge reamer can be used to discharge chips under the holes. The reamer parameters are shown in Table 5. The pilot holes were drilled by two-flute uncoated tungsten carbide twist drills with a diameter of 7.65 ± 0.003 mm. The wet machining was employed in the single-shot drilling to reduce the heat and mechanical damage to the pilot holes. The tolerances of the pilot holes were evaluated after drilling and strictly constrained between IT9 to IT10. The pre-drilling conditions are shown in Table 6.

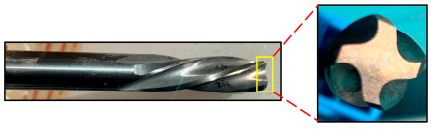

Figure 2. The reamer.

Table 5. Experimental conditions for reaming.

Item	Value
Rotation speed, n (rpm)	200, 400, 600, 800, 1000
Frequency, f (kHz)	21.5
Amplitude A (μm)	2, 4, 6
Reaming margin (mm)	0.15
Cutting condition	Dry cutting

Table 6. Drilling experimental conditions.

Item	Value
Drill bit	Uncoated tungsten carbide drill
Rotation speed in CFRP/Ti (rpm)	2000/700
Feed rate (mm/min)	20
Cutting condition	Drilling with coolant

In the preliminary experiment, the thrust forces and tool wear of CFRP and titanium alloys under different feeds were compared at 200 rpm. According to [22], the feed rate range of CFRP and the titanium alloy is 5, 10, 20, and 25 mm/min. Under these parameters, the CFRP is suitable for 25 mm/min feed and the titanium alloy is suitable for 10 mm/min feed. The feed speed of the two materials is more than three times different. In the case of a similar feed speed, only the smaller one can be used, which will reduce the efficiency of processing. It has been shown that a low feedrate should be used for UVR of Ti, but high feedrate could be used for UVR of CFRP [17]. In addition, using a variable feedrate led to a lower cutting force. Therefore, the experiments were carried out using different cutting parameters according to the different material properties, and lower thrust forces and higher machining efficiency were achieved compared to machining using the same parameters. In this experiment, a faster speed of 0.41 mm/s was used to ream holes in CFRP for machining and a slower speed of 0.16 mm/s for machining titanium alloys. Near the end of CFRP machining, the feedrate changes from 0.41 mm/s to 0.16 mm/s. The pattern of variation of feedrate with feed depth is shown in Figure 3. The other parameters used in the experiments are described in Tables 5 and 6. The error bars were based on three repetitions in each of the following groups.

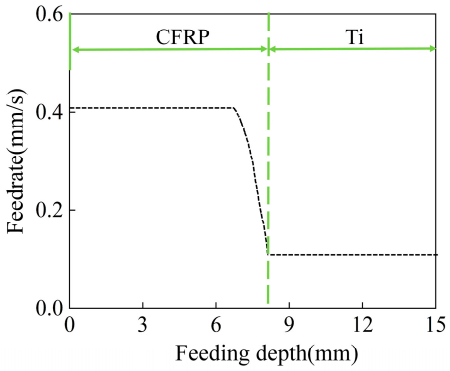

Figure 3. The feed rate varies with the feed depth.

A multicomponent dynamometer (9139AA, Kistler Instrumente AG, Winterthur, Switzerland) was used to measure the thrust force in experiments. The thrust force was converted into electrical signals by dynamometer, which were processed by a multichannel charge amplifier (5080A, Kistler Instrumente AG, Switzerland), converted, and transmitted to a computer through an analog to digital converter card (5697A1, Kistler Instrumente AG, Winterthur, Switzerland).

The hole quality was analyzed after reaming from aspects of geometric parameters (hole diameter, roundness), internal hole surface defects, the roughness of CFRP and titanium alloy holes, CFRP hole entrance, and exit morphology. The measurements of CFRP and titanium alloy hole diameter and roundness were performed using a coordinate measuring machine (PRISMO12020222, ZEISS, Oberkochen, Germany). CFRP and titanium alloy hole walls are measured, respectively. When measuring, 50 points are taken every week to fit the circle at the hole position every 1 mm. Average values are taken to obtain the hole diameter and roundness. The surface roughness of holes was measured with the Tyler Hopson surface profiler (CLI2000, Taylor Hobson Ltd., Leicester, UK). The roughness of CFRP and titanium alloys is measured separately. For the reliability of the results, the probe of the roughness analyzer runs through almost the entire pore size. The CFRP test length is 5.6 mm, and the titanium alloy test length is 6.6 mm. The optical microscope (OM; VHX-600E, KEYENCY, Osaka, Japan) was applied to observe the hole exit morphology. The inner wall morphology of the pores was observed with a scanning electron microscope (SU5000, Hitachi-hightech, Tokyo, Japan). The laser displacement sensor (OPTEX) is used to measure ultrasonic amplitude.

3. Results and Discussions

3.1. Analysis of Force Change and Amplitude Effect during Reaming

As shown in Figure 4, the motion of CR includes the rotation and axial feed motion of the reamer, while UVR is formed by applying longitudinal ultrasonic vibration to the motion of CR.

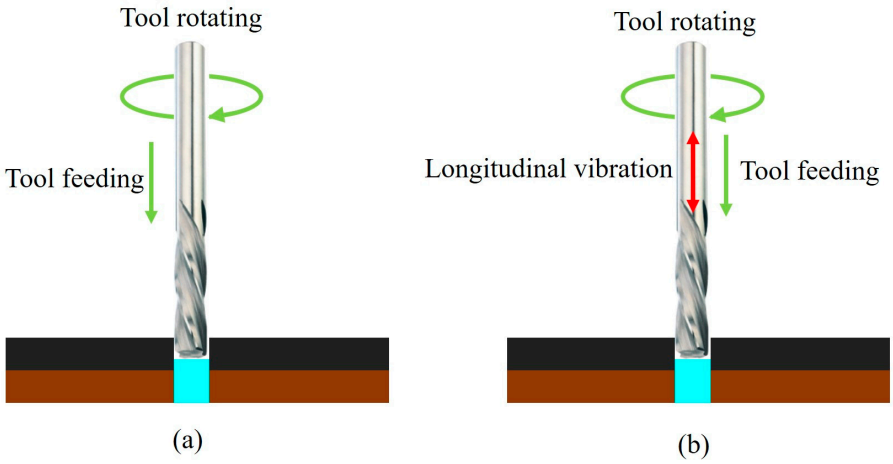

Figure 4. Diagram of reaming: (**a**) conventional reaming (CR); (**b**) ultrasonic vibration reaming (UVR).

In the reaming process, the reaming edge plays a main role. The reaming edge is long and only part of it is involved in cutting. When reaming CFRP/Ti stacks, it can be divided into six stages as a whole. As shown in Figure 5, stage I is the articulation stage and the beginning stage of reaming, during which the reamer edge contacts the CFRP surface. Stage II is the steady-state reaming stage of CFRP, in which the axial force of reaming gradually increases and enters the stable stage. Stage III enters the transition zone, which is the reaming stage of CFRP. Because of the difference of performance between the titanium alloy and CFRP, the reaming axial force rises sharply and enters the reaming stage of the titanium alloy. Stage IV is the steady-state reaming of the titanium alloy, in which the reaming axial force first rises and then enters the stable stage. Stage V is the end stage of titanium alloy reaming, in which the axial force of reaming decreases and the reaming stage approaches the end. Stage VI is the end stage of laminated reaming, in which the reaming axial force decreases to zero, the reamer edge hinges on the laminated holes, and the reaming process ends.

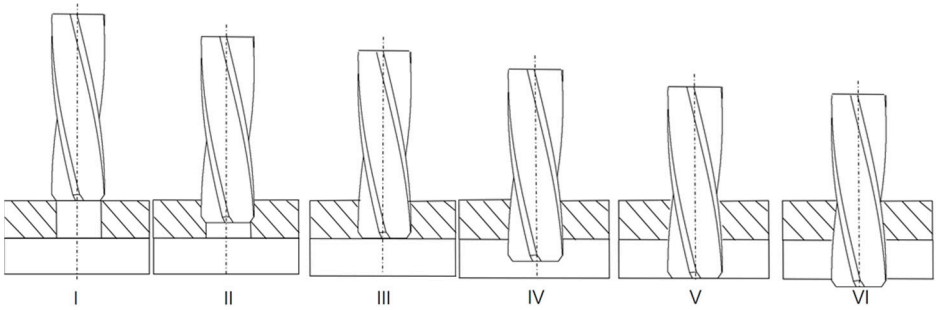

Figure 5. Schematic diagram of reaming process (I) Start of reaming (II) Cutting CFRP layer (III) End of CFRP reaming (IV) Reaming titanium alloy layer (V) Tool cutting edge contact interface (VI) End of reaming.

When the feed speed is 25 mm/min (CFRP) and 10 mm/min (titanium alloy), the tool speed is 1400 r/min, the amplitude of ultrasonic vibration is 6 μm, and the change of thrust force in reaming is collected. Time-domain signal analysis of reaming force is an effective method to reflect the real-time state of tool-workpiece interaction. Figure 6 is the cutting force curve of CFRP/Ti stacks during CR. It can be seen from the diagram that the thrust force in reaming presents five different stages. In stage A-B, the reamer gradually hinges into the CFRP layer, and the thrust force gradually increases. In the B-C stage, the reamer cutting edge is completely immersed in the CFRP layer material, i.e., in the stable cutting stage of the CFRP layer, and the cutting force remains stable. During the A-C stage, the titanium alloy is not involved in cutting, in which the titanium alloy acts as a simple support. After point C, the axial force decreases to some extent (stages C to C1), which is caused by the existence of voids between the titanium alloy and the CFRP layer material. Starting at point C1, the material is reamed from the reaming edge to the cutting edge, and the axial force increases sharply until the cutting edge is fully penetrated into the titanium alloy (stage C1-D). It can be seen that the axial force in reaming increases to 5–6 times that in the reaming of CFRP in a short time. Titanium alloy is an elastic plastic material with high tensile strength and low thermal conductivity, so its reaming force is relatively high. In stages D-E, the stable reaming stage is attained for the titanium alloy. In stage E-E1, the cutting edge of the reamer is gradually reamed out of the titanium alloy, and the axial force of reaming force decreases rapidly. At F, the reamer reaches the bottom of the hole. At the end of reaming, the axial force decreases to zero.

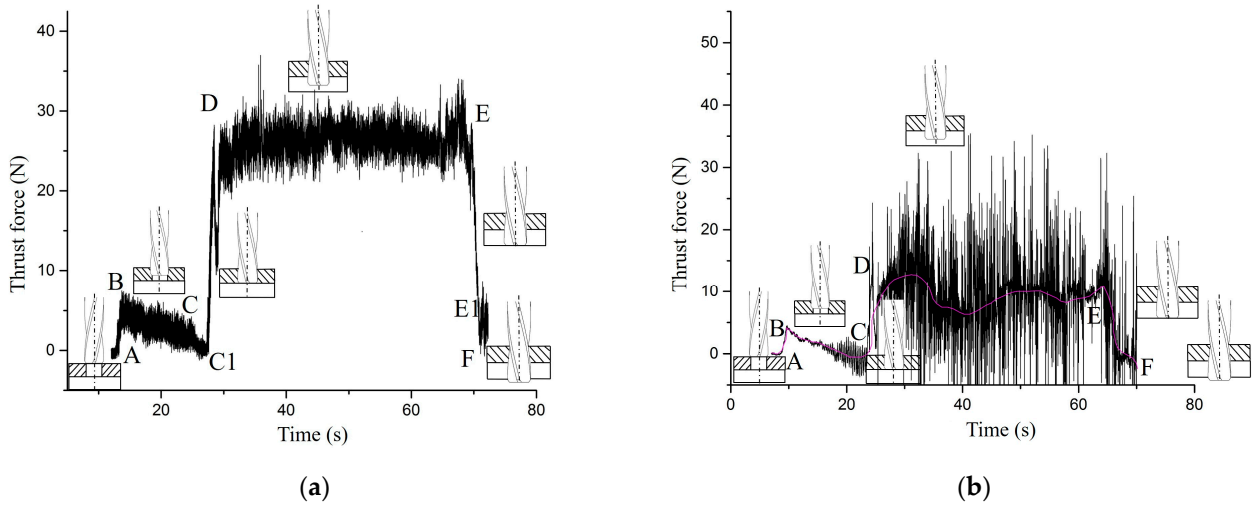

Figure 6. The thrust force of (**a**) CR and (**b**) UVR.

Figure 6 shows the thrust force curve obtained by UVR. It can be seen from the picture. UVR causes the large vibration of the reaming force. Compared with CR, the total reaming time is the same, but the proportion of the "empty cutting" process in ultrasonic vibration reaming reaches about 50%, and the average reaming thrust force of B-C and D-E stages is small. The thrust force of UVR is 40% smaller than CR in A-F stages. The average reaming axial forces—24 N of D-E stages in the stabilization stage of CR and 12 N in the D-E stages of UVR—are lower than the former by 50%. This is mainly due to the fact that during UVR, the chips are all debris-like and the process of removing the outside of the hole along the chip guide groove is relatively smooth. In addition, in ultrasonic vibration reaming, the reamer has been in the state of "empty cutting" for a long time, while the cutting edge of the reamer has been in the state of cutting in CR. This is consistent with the trend of force variation in ultrasonic assisted drilling. However, due to the large cutting thickness in drilling, the extrusion of the cutting edge on the hole wall limits the exertion of ultrasonic effect. In ultrasonic reaming, the effect of ultrasound is obvious because of the small cutting thickness; thus, the effect of reducing force is more obvious.

Taking the selectable points on the tool as the research object, the motion equation of ordinary hinge cutting is as follows:

$$\begin{cases} x = \frac{D}{2}\cos(2\pi nt/60) \\ y = \frac{D}{2}\sin(2\pi nt/60) \\ z = v_a t \end{cases} \quad (1)$$

In Formula (1), v_a is the feed speed of the spindle. During ultrasonic reaming, ultrasonic vibration is applied axially and the equation of trajectory motion changes to

$$\begin{cases} x = \frac{D}{2}\cos(2\pi nt/60) \\ y = \frac{D}{2}\sin(2\pi nt/60) \\ z = v_a t + A\sin(2\pi ft) \end{cases} \quad (2)$$

In Equation (2), A is the ultrasonic amplitude and f is the ultrasonic vibration frequency. Figure 7a shows the trajectories of the selectable points on the main cutting edge of the reamer of CR and Figure 7b shows that of UVR.

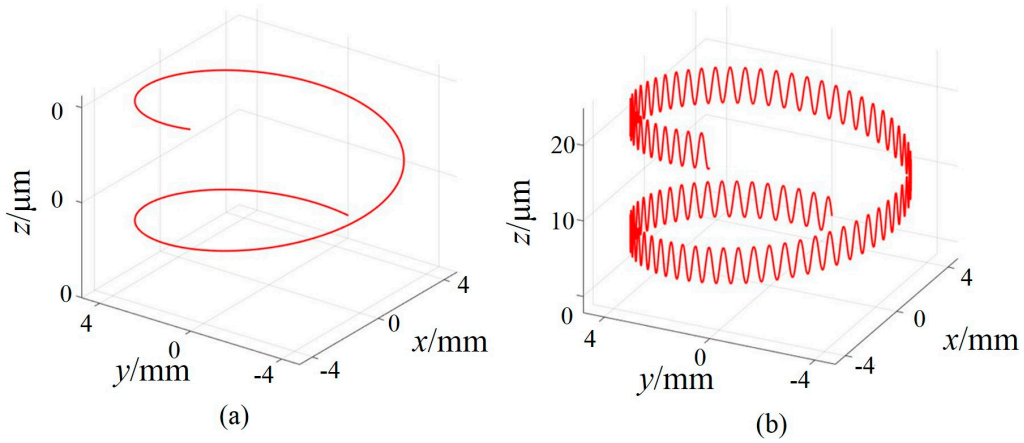

Figure 7. Cutting trajectory of the selectable points on the cutting edge of the reamer: (**a**) CR; (**b**) UVR.

In UVR for this test, the equation of motion tracking for the four-edged reamer blade on the hole wall during reaming is:

$$\begin{cases} Z_A(\theta) = \frac{f_z}{2\pi}\theta + A\sin(W_f\theta) \\ Z_B(\theta) = \frac{f_z}{2\pi}(\theta+\pi) + A\sin[(W_f(\theta+\frac{\pi}{2})] \\ Z_C(\theta) = \frac{f_z}{2\pi}(\theta+\pi) + A\sin[(W_f(\theta+\pi)] \\ Z_D(\theta) = \frac{f_z}{2\pi}(\theta+\pi) + A\sin[(W_f(\theta+\frac{3\pi}{2})] \\ W_f = \frac{60f_z}{n} \end{cases} \quad (3)$$

In Formula (3), Z_A, Z_B, Z_C, and Z_D are the displacements of each cutting edge in the feed direction with the angle of rotation of the reamer. The feed quantity per tooth of the tool is f_z. W_f represents the number of vibrations per rotation of the reamer. It can be obtained from Formula (3). The axial thickness between the two cutting edges is expressed as follows:

$$\begin{array}{l} f_1 = \frac{f}{4} + 2A\sin(\frac{W_f}{2}\pi)\cos[W_f(\theta+\frac{(2k-1)\pi}{4})] \\ (k = 1,2,3,4) \end{array} \quad (4)$$

The phase difference between the two blades when vibration occurs is:

$$\Phi = \frac{\pi}{2}W_f \quad (5)$$

Minimum cutting thickness in the axial direction of both blades is:

$$f_{t'} = \frac{f}{4} - 2A\left|\sin(\frac{W_f}{4}\pi)\right| \quad (6)$$

It can be seen from Equation (6) that the cutting thickness is related to the amplitude and feed. The greater the amplitude A, the more obvious the chip breaking effect is. Chips press the front face intermittently, reducing sliding friction. Therefore, the larger the amplitude, the smaller the thrust force.

3.2. Thrust Forces

Figure 8 shows the variation of thrust force with ultrasonic amplitude through the two materials during the reaming of CFRP/Ti stacks by UVR. In the experiment, the tool speed was 600 rpm, and the feed speed was 0.41 mm/s (CFRP) and Ti (0.16 mm/s). During the reaming of the titanium alloy, the thrust force decreases with the increase of ultrasonic amplitude and reaches its minimum value when the amplitude reaches 6 μm, which is 19 N less than the thrust forces of CR. In the reaming of CFRP, the thrust forces also decrease with the increase of ultrasonic amplitude and reach their minimum value when the amplitude reaches 6 μm, which is 4 N less than thrust forces of CR. The average thrust forces in UVR decreased by 57% (Ti) and 40% (CFRP), respectively, compared to CR. Therefore, the larger the amplitude, the smaller the axial force. This is consistent with the analysis in Section 3.1.

According to [23],

$$F_{mcr} = k_{cr}v_a a_p \quad (7)$$

$$F_{mar} = \frac{t_e - t_b}{T}k_{ar}v_a a_p \quad (8)$$

where k_{cr} and k_{ar} are the specific resistances in the axial thrust direction for CR and UVR, respectively. a_p is the depth of cut, the thrust force in CR is F_{mcr}, the thrust force in UVR is F_{mar}, and the vibration period of UVR is T. Frictional direction between the rake face of the tool and the chip is reversed at t_i. The UVR starts at t_b and ends at t_e. Therefore, $(t_e - t_b)/T < 1$, $F_{mar} < F_{mcr}$, yielding smaller thrust forces for UVR.

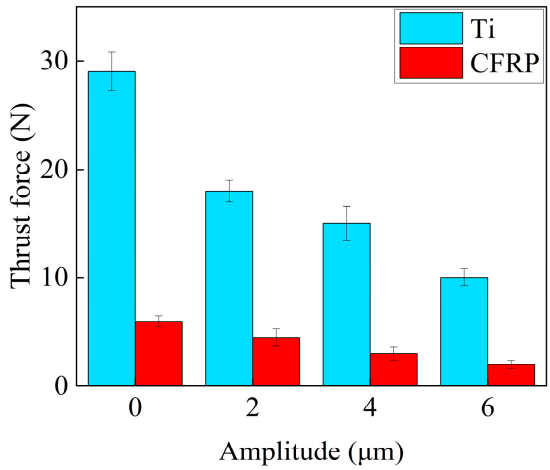

Figure 8. Comparison of thrust forces at different ultrasonic amplitudes.

Figure 9 depicts the variation in thrust force with respect to tool speed. In the experiment, the ultrasonic amplitude was 6 μm. The thrust forces when machining CFRP and titanium alloys by UVR are lower than CR. When reaming the titanium alloy, the trend of thrust force reduction with the increase of tool speed increases and then stabilizes, which means that when the speed is low, the thrust forces are larger and the effect of ultrasonic in reducing thrust force is not obvious. As the speed increases, the ultrasonic effect becomes more and more obvious, and when the speed reaches 1400 rpm, the thrust forces of CR no longer decrease and become stable. At that speed, the effect of ultrasonic thrust force reduction is also stable. The higher the rotation speed, the smaller the reamer feed per tooth, the weaker the suppression of ultrasound by sidewall extrusion, and the smaller the thrust force, indicating that the ultrasound effect is better.

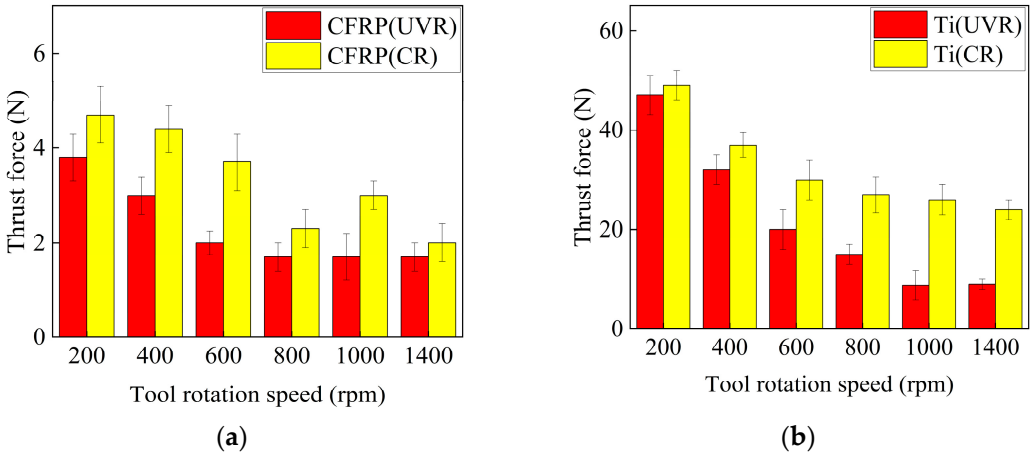

Figure 9. Comparison of thrust forces at different levels of tool rotation speed: (**a**) CFRP; (**b**) Ti.

3.3. Roughness

Figure 10 illustrates the distribution of hole wall roughness for CFRP and titanium alloy at different rotational speeds. In the experiment, the ultrasonic amplitude was 6 μm. It is concluded that when the rotational speed is lower, the difference between the hole wall roughness of UVR and CR is larger. When the rotational speed is 200 rpm, the roughness of CFRP is reduced by 20% with UVR and 28% for the titanium alloy, which indicates that ultrasonic improves the hole wall roughness of the laminated material better at low rotational speed machining parameters. As the rotational speed increases, the hole wall roughness decreases for both CR reaming and UVR. It shows that the higher the rotational speed, the better the hole wall finish. The reason for this phenomenon is that the reamer

side edge scrapes the hole wall more significantly due to the higher reamer feed per tooth at lower speeds. As a result, ultrasound is more effective in improving roughness.

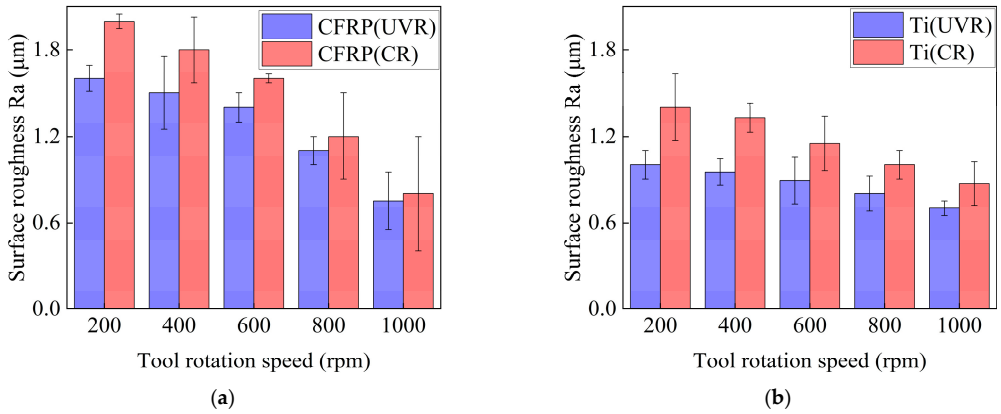

Figure 10. Comparison of surface roughness at different levels of tool rotation speed: (**a**) machined CFRP surface; (**b**) machined Ti surface.

3.4. Diameter and Roundness

The variation in hole diameter with rotational speed during the reaming process using UVR and CR is shown in Figure 11, where the reamer diameter is 7.8 mm. In the experiment, the ultrasonic amplitude was 6 μm. The hole diameter of CFRP and the titanium alloy machined by UVR is within the H7 tolerance band, and, by CR, it is within the H8 tolerance band, which is worse compared to UVR. The reliability of the UVR process was verified by comparing the average hole diameter during the reaming process. When reaming CFRP by CR, as the speed increases, more cutting heat is generated, the hole diameter increases, and the error becomes larger. At the same speed (200 rpm and 400 rpm), the increase in hole diameter of CFRP is smaller compared to that of the titanium alloy because the elastic recovery of the holes after reaming of CFRP reduces the hole diameter, which weakens the increase in hole diameter due to cutting heat.

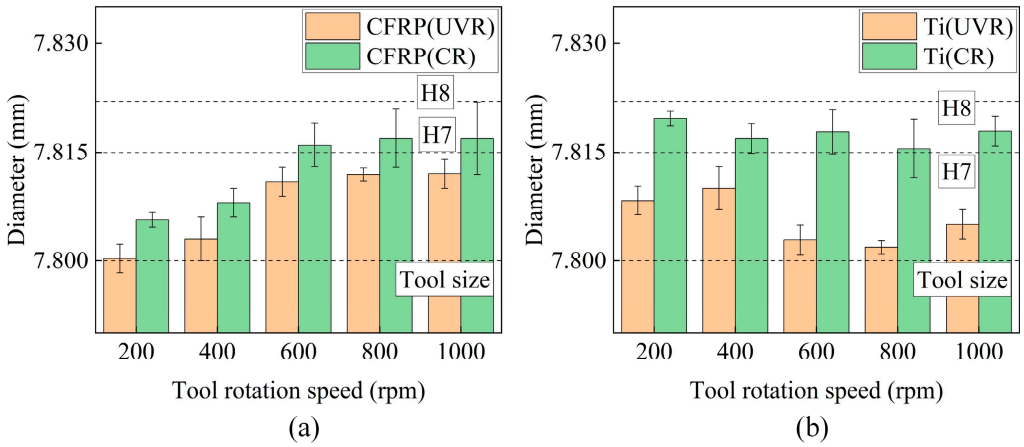

Figure 11. Comparison of diameter at different levels of tool rotation speed: (**a**) machined CFRP surface; (**b**) machined Ti surface.

Figure 12 demonstrates the variation in roundness with speed for CFRP/Ti stacked holes. In the experiment, the ultrasonic amplitude was 6 µm. The average error in roundness by UVR is 0.01 mm smaller than that of CR. The error of using UVR is on average 0.015 mm smaller than that of using CR, indicating that UVR results in a hole that is closer to round. This is because ultrasonic reaming reduces the heat generated during the reaming process, thus reducing thermal damage and deformation and making the hole closer to round.

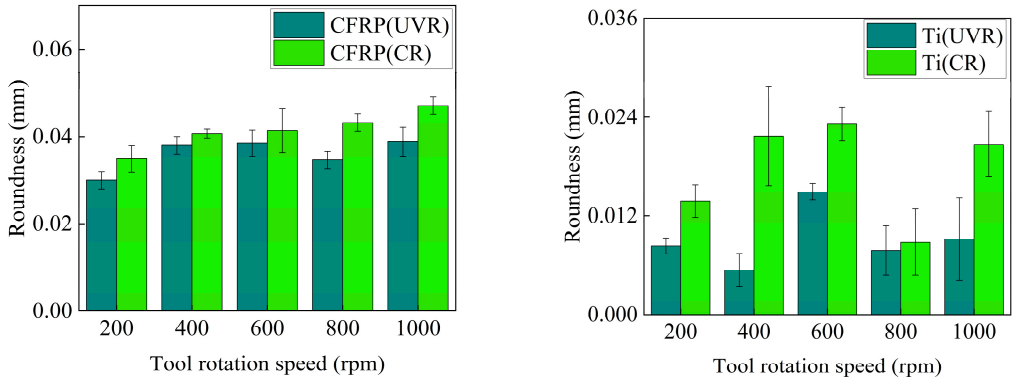

Figure 12. Comparison of roundness at different levels of tool rotation speed: (**a**) machined CFRP hole; (**b**) machined Ti hole.

3.5. The Quality of Entrances and Exits

Figure 13 displays the surface appearance of the exit and entrance of the CFRP normally reamed hole and the ultrasonically reamed hole at a rotational speed of 600 rpm. In the experiment, the ultrasonic amplitude was 6 µm. The entrance of the ultrasonic reamed hole is relatively smooth, and the surface produces less fiber pull-out. However, the hole of CFRP has more fiber pull-out and more fiber protrusion at the exit of CR. When ultrasound was applied, the exit defects of CFRP were significantly reduced, indicating that UVR is effective in improving the surface quality of CFRP entrance and exit. The reason for this result is that the ultrasonic vibration of the reamer cutting edge helps to remove the carbon fibers by shear fracture mode and the surface quality of CFRP exit and entrance is improved.

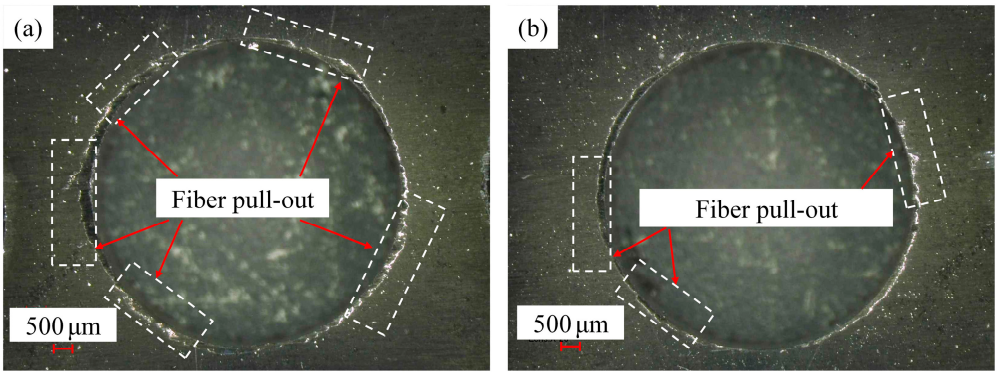

Figure 13. *Cont.*

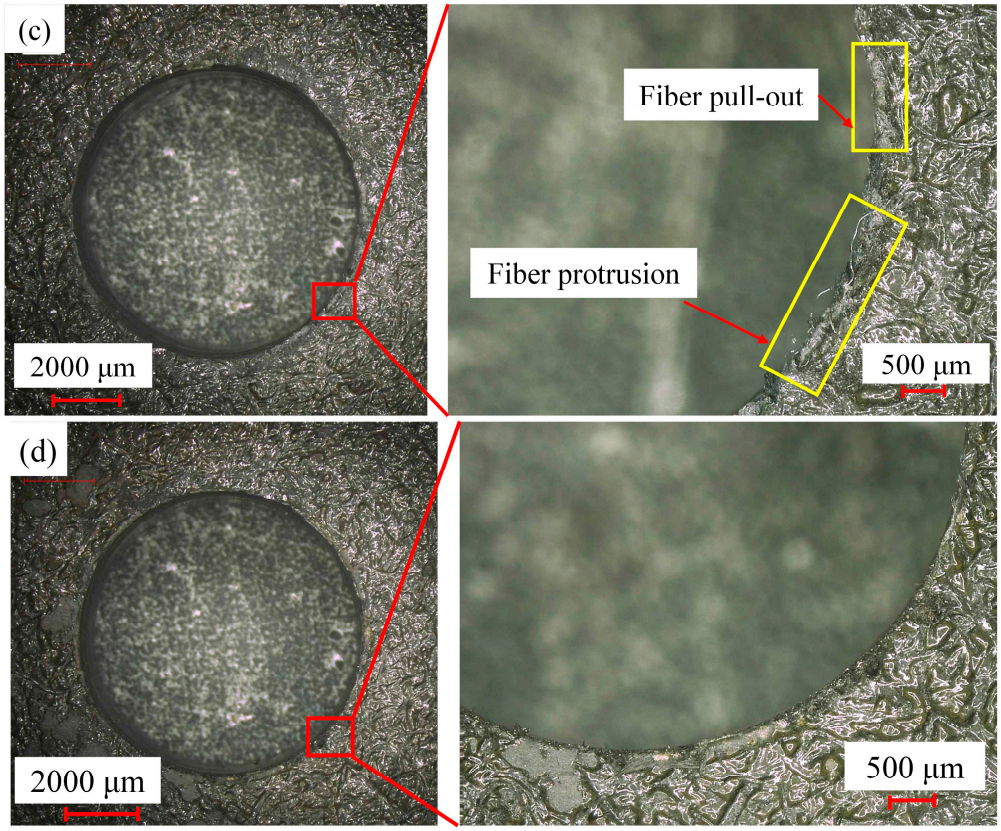

Figure 13. Surface morphology of CFRP: (**a**) entrances in CR; (**b**) entrances in UVR; (**c**) exit in CR; (**d**) exit in UVR.

Figure 14 presents the surface appearance of the entrances and exits of the titanium alloy by CR and UVR. At a rotational speed of 600 rpm, the entrances machined by CR have chipping. In the experiment, the ultrasonic amplitude was 6 μm. In contrast, the entrances machined by UVR have a complete surface. When the reamer enters the CFRP-titanium alloy interface, the reamer is subjected to force fluctuations that cause damage to the area. The ultrasonic action reduces the cutting temperature, which makes the exit surface of the titanium alloy more complete than that of CR.

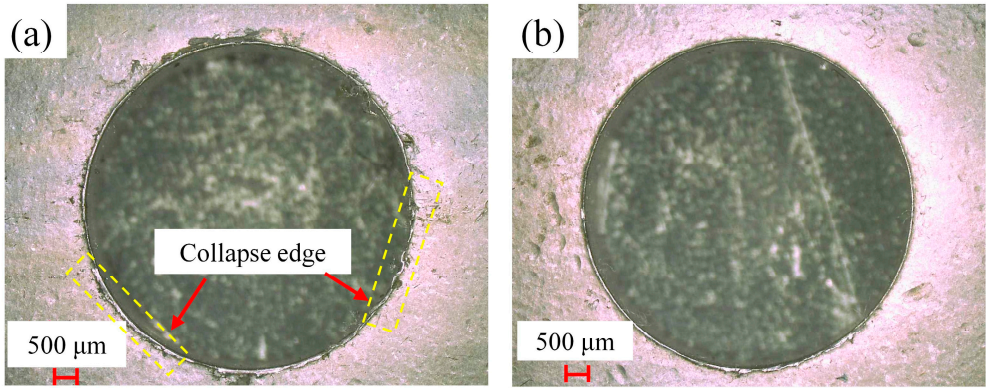

Figure 14. *Cont.*

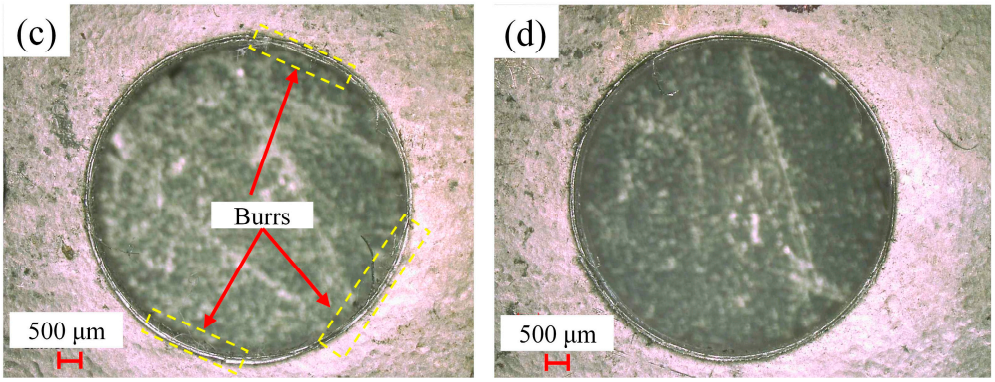

Figure 14. Surface morphology of titanium alloy: (**a**) entrances in CR; (**b**) entrances in UVR; (**c**) exit in CR; (**d**) exit in UVR.

3.6. Hole Quality

CFRP is a typical anisotropic material, which is different from the titanium alloy and belongs to isotropic material with simple influence law. Different layers of CFRP have different material removal during cutting due to the influence of the fiber cutting angle. Figure 15 is a schematic diagram of material removal corresponding to the angle between 0 and 180°.

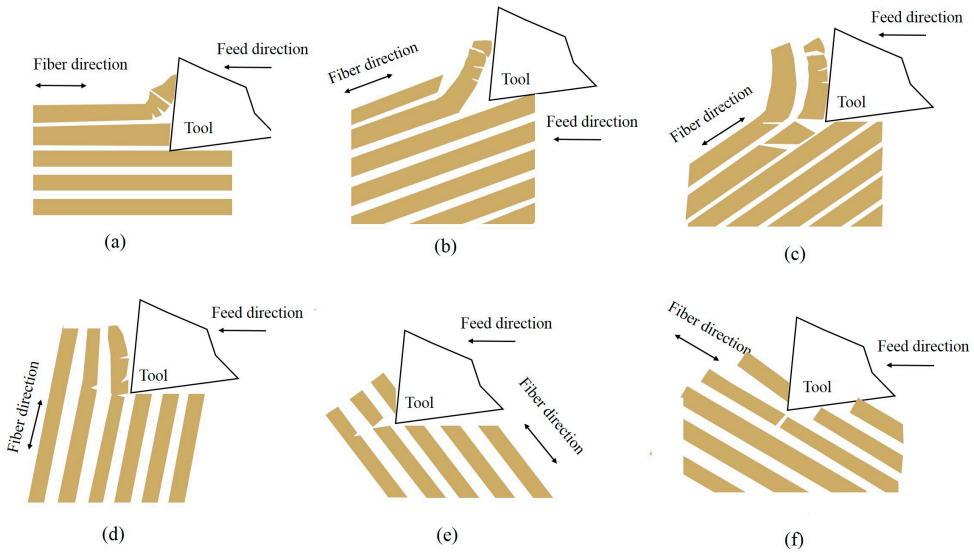

Figure 15. Material removal diagrams corresponding to the angle between 0 and 180°. (**a**) θ =0°/180° (**b**) θ =15° (**c**) θ =40° (**d**) θ =70° (**e**) θ =120° (**f**) θ =150°.

CFRP laminates are composed of carbon fibers and resin matrix, which determine the main material breakage is fiber/resin debonding and fiber breakage. Carbon fibers are mainly brittle before fracture. Fiber/resin debonding occurs close to the 0/180° fiber cutting angle area. As shown in Figure 16a,b, carbon fibers are fully exposed to the machined surface during ordinary reaming. Some carbon fibers break along the transverse direction because when the fibers/resins are debonded, they break after bending to a certain extent. It can also be seen that a small portion of the fibers break lengthwise due to the extrusion of the carbon fibers under the action of the cutting edge and the flank face. Figure 16c is a break diagram of CFRP fibers under ultrasonic reaming, from which it can be seen that the exposed fibers show significantly less transverse breakage and no longitudinal breakage.

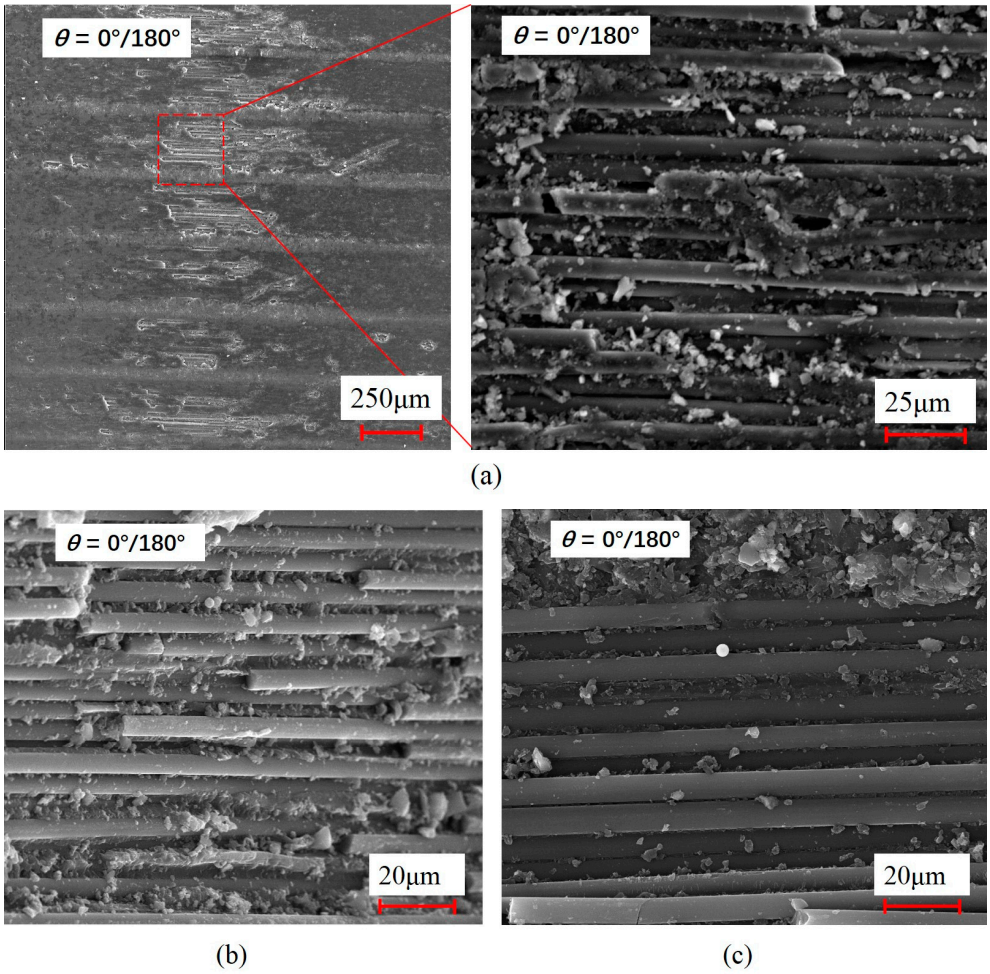

Figure 16. Diagram of 0/180° fiber cutting angle: (**a**) CR; (**b**) CR; (**c**) UVR.

When the angle of cut of the fiber angle is 15°, the surface morphology is 3000 times larger under the scanning electron microscope, as shown in Figure 17. From Figure 17a, it can be seen in the fracture diagram of ordinary reamed fibers that the fiber fracture is parallel to the cutting surface. From 5000 times magnification of local fibers, the roughness of the fracture surface can be observed, and extrusion fracture of the fibers is obvious. In addition, some of the carbon fibers were exposed to the surface, indicating that there was also a fiber/resin debonding fracture. When the cutting edge direction of the reamer is the opposite to that of fiber, the debonding and fracture of fiber/resin occurs under the push of cutting edge, but it is shorter than the cutting angle of 0/180°. A recess in Figure 17a indicates a very uneven breakage during ordinary reaming. Figure 17b shows the breakage pattern of fibers during ultrasonic reaming. Compared with ordinary reaming, the breakage is uniform, and the cross section is smooth.

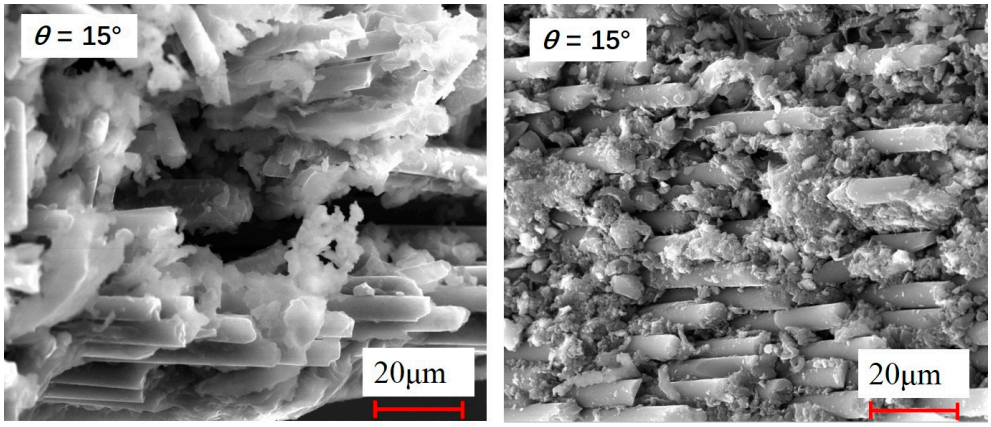

Figure 17. Diagram of 15° fiber cutting angle: (**a**) CR; (**b**) UVR.

The area with the most surface pits occurs near the cutting angle of the fibers at 40°, as shown in Figure 18a. With ordinary reaming, the machined surface is serrated, and the surface quality is poor. The pit is the main cause of the formation of the serrated surface. It can be observed from the fracture surface that three fracture modes exist and alternate, including fiber shear fracture, fiber bending fracture, and fiber/resin debonding. Figure 18b shows the shape of the machined surface during ultrasonic reaming. It can be seen that the fiber/resin debonding phenomenon is significantly reduced, the serrated shape is more uniform, and the pit fluctuation is smaller than that of ordinary reaming. As the surface quality at the cutting angle of this fiber is the worst, it is the main reason for the formation of the hole wall morphology.

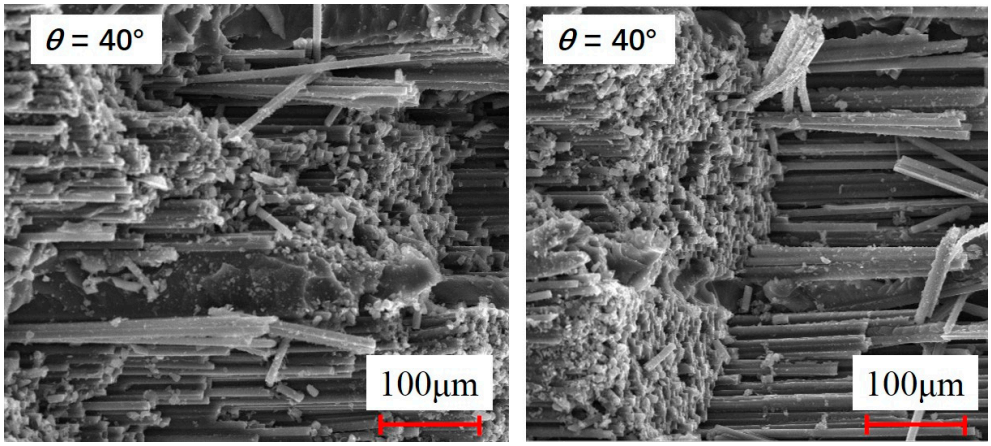

Figure 18. Diagram of 40° fiber cutting angle: (**a**) CR; (**b**) UVR.

As shown in Figure 19, the 70° fiber angle, observed 8000 times larger under scanning electron microscopy, indicates the morphology, which is typical of fiber bending fracture and partial extrusion fracture. It can be seen from the diagram that the form of the fiber/resin debonding fracture is limited, so the depth of defects in this surface layer is very limited, and most of the fiber fracture is caused by bending fracture. Figure 19a is the morphology of ordinary reaming. It can be seen that the fiber fracture is rough and uneven, and there are many "round holes", which are caused by uneven pull-out height of the fiber due to uneven bending and fracture. Figure 19b shows the morphology during ultrasonic reaming. It can be observed that the surface of carbon fiber fracture is relatively flat and the number of "round holes" is less than that of ordinary reaming. It shows that the bending

fracture of the fiber is more uniform, and the pull-out height difference is smaller under the ultrasonic-assisted reaming.

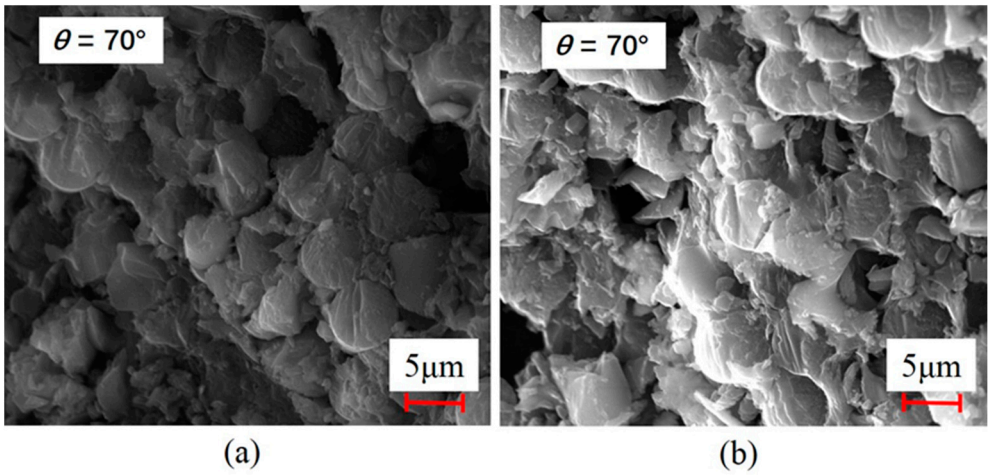

Figure 19. Diagram of 70° fiber cutting angle: (**a**) CR; (**b**) UVR.

Figure 20 is the morphology observed at a 120° fiber angle. The shear fracture of the fibers plays a major role, resulting in smooth and flat surface fracture of most carbon fibers. The surface dominated by fiber shear has almost no secondary surface defects and has the lowest roughness of all fiber cutting angles (Figure 20a). The evenly broken fiber section can be observed when reaming is 4000 times larger than that under SEM. Figure 20b is the morphology observed when reaming under SEM, 4000 times larger. The end surface of the fiber is smooth and flat.

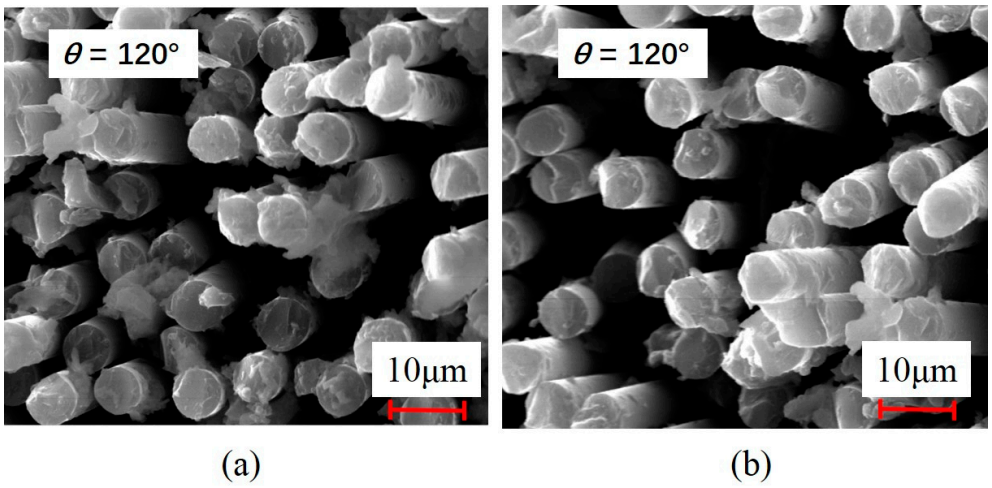

Figure 20. Diagram of 120° fiber cutting angle: (**a**) CR; (**b**) UVR.

The morphology of Figure 21 is observed when the cutting angle of the fibers is around 150°. Figure 21a is the morphology of ordinary reaming. It can be seen that most of the breaks of carbon fibers are transversely broken along the fibers due to the extrusion of carbon fibers by the cutting edge of the reamer. The debonding breakage of fibers and resins also causes some of the outer surfaces of carbon fibers to be exposed outside the cutting surfaces. Fiber ports are unevenly arranged, with many small segments, not completely cut off, connected to the fiber head, resulting in poor surface roughness. Figure 21b shows the morphology during ultrasonic reaming. Similar to ordinary reaming, there are many fiber breaks of different lengths, but these breaks are flatter than with ordinary reaming, and the roughness is significantly improved with ordinary reaming.

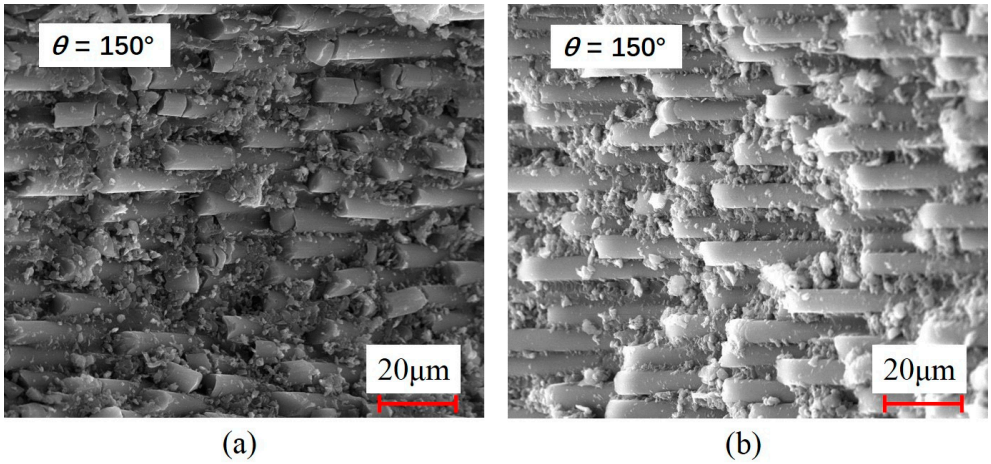

Figure 21. Diagram of 150° fiber cutting angle: (**a**) CR; (**b**) UVR.

Figure 22a is a plot of the inner wall of a common-reaming titanium alloy when the tool speed was 600 rpm and the ultrasonic amplitude was 6 μm, observed under a scanning electron microscope. It can be seen that there are flat marks on this inner wall; this is due to the fact that there is only feed speed in the axial direction. A portion in the spiral from the MATLAB simulation is an approximate straight line. Figure 22b is a plot of the inner wall of the ultrasonic titanium alloy observed under SEM when the tool speed is 600 rpm, and it can be seen that there are wave scratches on the inner wall, which are due to the added ultrasonic vibration on the axial feed. A portion of the spiral curve taken from the MATLAB simulation plot is an approximate wave line. The actual scratches under both machining conditions are consistent with the MATLAB simulation.

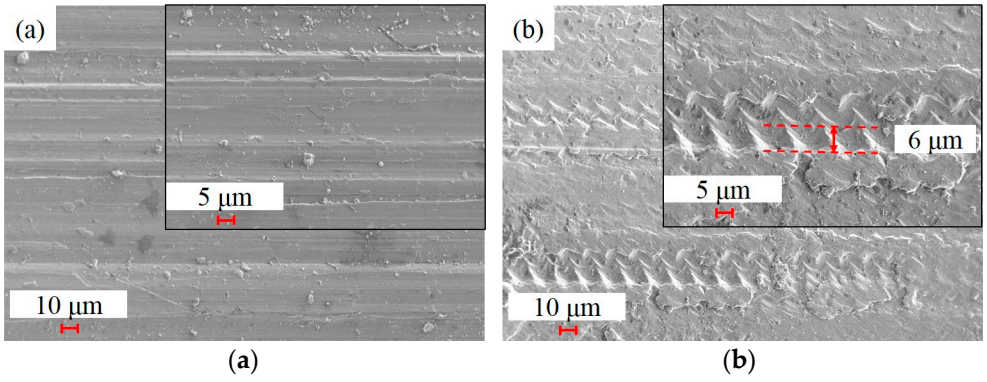

Figure 22. SEM images of Ti hole wall drilled by: (**a**) CR; (**b**) UVR.

4. Conclusions

In this study, experiments on the UVR of CFRP/Ti stacks were conducted. The experiments studied the influence of different ultrasonic amplitudes on reaming thrust and the influence of tool speed on thrust, dimensional accuracy, and surface roughness under optimal ultrasonic amplitude:

(1) UVR can reduce the roughness of CFRP/Ti stacked holes, improve diameter and roundness, reduce entrance and exit defects of laminated holes, and improve the quality of holes. Therefore, UVR is an effective finishing method;

(2) At the same rotational speed, the higher the ultrasonic output power, the more obvious the reduction in thrust forces. When the amplitude reaches 6 μm, the average thrust forces in UVR were decreased by over 57% (titanium alloy) and 40% (CFRP), respectively, compared to CR. At different tool rotational speeds, the thrust force at

UVR is less than CR when machining CFRP/Ti stacks. When the rotational speed is higher, the thrust force is reduced more dramatically;

(3) The surface roughness of holes for CFRP and the titanium alloy fabricated by UVR is less than that by CR. In addition, the difference with CR is more obvious under the condition of lower tool rotational speed. When the rotational speed is 200 rpm, the roughness of CFRP is reduced by 20% with UVR and 28% for the titanium alloy;

(4) With the introduction of ultrasound, the diameter difference between CFRP (around 11 μm (CR) vs. 7 μm (UVR)) and the titanium alloy (around 17 μm (CR) vs. 5 μm (UVR)) holes becomes smaller. CFRP/Ti stacked holes machined by UVR have better roundness than those by CR;

(5) With CR, the hole of CFRP has fiber pullout and more fiber protrusion at the entrance/exit, while it has fewer defects with UVR. There are burrs and chippings at the entrance and exit of the titanium alloy with CR, while burrs and chippings can be reduced with UVR. Fiber arrangement of CFRP hole walls is uniform by UVR, whereas fiber breakage occurs by CR;

(6) UVR is a effective method for reaming CFRP/Ti stacked holes. Concerning the change of feed speed with material, 1000 rpm is more advantageous to the reduction of thrust force and the improvement of surface roughness. Tool speed selection at 600 rpm is more conducive to the reduction of hole size error. Tool speed is selected at 800 rpm, which is favorable for keeping the roundness of hole diameter.

Author Contributions: Conceptualization, Y.W. and S.L.; methodology, Y.W.; software, Y.Q.; validation, R.K., Z.D. and X.G.; formal analysis, Y.W.; investigation, S.L.; resources, Z.D.; data curation, Y.W.; writing—original draft preparation, S.L.; writing—review and editing, Z.D.; visualization, R.K.; supervision, X.G.; project administration, R.K.; funding acquisition, R.K. All authors have read and agreed to the published version of the manuscript.

Funding: This research was funded by National Natural Science Foundation of China (Grant No. U20A20291), High Level Talents Innovation Plan of Dalian (Grant No. 2020RD02).

Institutional Review Board Statement: Not applicable.

Informed Consent Statement: Not applicable.

Data Availability Statement: Not applicable.

Acknowledgments: Thank you very much for the funding of National Natural Science Foundation of China fund and High Level Talents Innovation Plan of Dalian. All the authors are greatly acknowledged for their financial support in making this research possible.

Conflicts of Interest: The authors declare no conflict of interest.

References

1. Wang, B.; Zhao, H.; Zhang, F.; Wang, M.; Zheng, Y. Comparison of the geometric accuracy of holes made in CFRP/Ti laminate by drilling and helical milling. *Int. J. Adv. Manuf. Technol.* **2021**, *112*, 3343–3350. [CrossRef]
2. Teti, R.; Segreto, T.; Caggiano, A.; Nele, L. Smart Multi-Sensor Monitoring in Drilling of CFRP/CFRP Composite Material Stacks for Aerospace Assembly Applications. *Appl. Sci.* **2020**, *10*, 758. [CrossRef]
3. Hu, W.; Du, P.; Qiu, X.; Zhao, X.; Hu, Z.; Zhang, J.; Liu, Y. Enhanced dry machinability of TC4 titanium alloy by longitudinal-bending hybrid ultrasonic vibration-assisted milling. *J. Clean. Prod.* **2022**, *379*, 134866. [CrossRef]
4. Shyha, I.S.; Soo, S.L.; Aspinwall, D.K.; Bradley, S.; Perry, R.; Harden, P.; Dawson, S. Hole quality assessment following drilling of metallic-composite stacks. *Int. J. Mach. Tools Manuf.* **2011**, *51*, 569–578. [CrossRef]
5. Yaşar, N.; Korkmaz, M.E.; Gupta, M.K.; Boy, M.; Günay, M. A novel method for improving drilling performance of CFRP/Ti6AL4V stacked materials. *Int. J. Adv. Manuf. Technol.* **2021**, *117*, 653–673. [CrossRef]
6. Kolesnyk, V.; Peterka, J.; Alekseev, O.; Neshta, A.; Xu, J.; Lysenko, B.; Sahul, M.; Martinovič, J.; Hrbal, J. Application of ANN for Analysis of Hole Accuracy and Drilling Temperature When Drilling CFRP/Ti Alloy Stacks. *Materials* **2022**, *15*, 1940. [CrossRef]
7. Gao, Y.; Yang, X.; Xiao, J.; Zhang, H. The development of an ultrasonic vibration hand-held pneumatic drill for hole-machining on CFRP composite materials. *Int. J. Adv. Manuf. Technol.* **2021**, *114*, 1635–1652. [CrossRef]
8. Xu, J.; El Mansori, M. Numerical studies of frictional responses when cutting hybrid CFRP/Ti composite. *Int. J. Adv. Manuf. Technol.* **2016**, *87*, 657–675. [CrossRef]

9. Kong, L.; Gao, D.; Lu, Y.; Jiang, Z. Novel orbital drilling and reaming tool for machining holes in carbon fiber–reinforced plastic (CFRP) composite laminates. *Int. J. Adv. Manuf. Technol.* **2020**, *110*, 977–988. [CrossRef]
10. Franz, G.; Vantomme, P.; Hassan, M.H. A Review on Drilling of Multilayer Fiber-Reinforced Polymer Composites and Aluminum Stacks: Optimization of Strategies for Improving the Drilling Performance of Aerospace Assemblies. *Fibers* **2022**, *10*, 78. [CrossRef]
11. Ahmed, S.; Kumar, P. Performance evaluation of cryogenic cooling in reaming titanium alloy. *Mater. Manuf. Process.* **2017**, *32*, 302–308. [CrossRef]
12. Isbilir, O.; Ghassemieh, E. Comparative study of tool life and hole quality in drilling of CFRP/titanium stack using coated carbide drill. *Mach. Sci. Technol.* **2013**, *17*, 380–409. [CrossRef]
13. Peltier, L.; Perroud, O.; Moll, P.; Slowensky, J.; Charbonnier, P.; Eberhardt, A.; Hautcoeur, A. Production and Mechanical Properties of Cu-Al-Ni-Be Shape Memory Alloy Thin Ribbons Using a Cold Co-Rolled Process. *Shape Mem. Superelasticity* **2021**, *7*, 344–352. [CrossRef]
14. An, Q.; Zhong, B.; Wang, X.; Zhang, H.; Sun, X.; Chen, M. Effects of drilling strategies for CFRP/Ti stacks on static mechanical property and fatigue behavior of open-hole CFRP laminates. *J. Manuf. Process.* **2021**, *64*, 409–420. [CrossRef]
15. Jiao, F.; Li, Y.; Niu, Y.; Zhang, Z.; Bie, W. A review on the drilling of CFRP/Ti stacks: Machining characteristics, damage mechanisms and suppression strategies at stack interface. *Compos. Struct.* **2023**, *305*, 116489. [CrossRef]
16. Jiang, Z.; Wang, F.; Zeng, D.; Zhu, S.; Fu, R. In-Process Tool Condition Forecasting of Drilling CFRP/Ti Stacks Based on ResNet and LSTM Network. *Appl. Sci.* **2023**, *13*, 1881. [CrossRef]
17. Cong, W.; Pei, Z.; Deines, T.; Liu, D.; Treadwell, C. Rotary ultrasonic machining of CFRP/Ti stacks using variable feedrate. *Compos. Part B Eng.* **2013**, *52*, 303–310. [CrossRef]
18. Gao, H.; Sun, C.; Ran, C.; Zhang, X.; Li, L. Experimental study on ultrasonic vibration assisted spiral milling of laminated composite materials. *J. Mil. Eng.* **2015**, *36*, 2342–2349.
19. Ma, G.; Kang, R.; Yin, S.; Wang, Y.; Dong, Z. Effect of amplitude ratios on hole quality in longitudinal–torsional coupled ultrasonic-assisted drilling of CFRP composites. *Int. J. Adv. Manuf. Technol.* **2022**, *122*, 2911–2926. [CrossRef]
20. Ma, G.; Kang, R.; Dong, Z.; Yin, S.; Bao, Y.; Guo, D. Hole quality in longitudinal–torsional coupled ultrasonic vibration assisted drilling of carbon fiber reinforced plastics. *Front. Mech. Eng.* **2020**, *15*, 538–546. [CrossRef]
21. Ma, G.; Kang, R.; Yan, C.; Bao, Y.; Zhu, X.; Dong, Z. Mechanical model of thrust force and torque in longitudinal-torsional coupled ultrasonic-assisted drilling of CFRP. *Int. J. Adv. Manuf. Technol.* **2021**, *119*, 189–202. [CrossRef]
22. Geng, D.; Zhang, D.; Li, Z.; Liu, D. Feasibility study of ultrasonic elliptical vibration-assisted reaming of carbon fiber reinforced plastics/titanium alloy stacks. *Ultrasonics* **2017**, *75*, 80–90. [CrossRef] [PubMed]
23. Ma, C.X.; Shamoto, E.; Moriwaki, T. Study on the Thrust Cutting Force in Ultrasonic Elliptical Vibration Cutting. *Mater. Sci. Forum* **2004**, *471–472*, 396–400. [CrossRef]

Disclaimer/Publisher's Note: The statements, opinions and data contained in all publications are solely those of the individual author(s) and contributor(s) and not of MDPI and/or the editor(s). MDPI and/or the editor(s) disclaim responsibility for any injury to people or property resulting from any ideas, methods, instructions or products referred to in the content.